Astron. Astrophys. 189, 243–253 (1988)

ASTRONOMY AND ASTROPHYSICS

NLTE effects in solar magnetic fluxtubes

S.K. Solanki [1] **and W. Steenbock** [2,*]

[1] Institute of Astronomy, ETH-Zentrum, CH-8092 Zürich, Switzerland
[2] Institut für Theoretische Physik und Sternwarte der Universität, Olshausenstrasse 40, D-2300 Kiel, Federal Republic of Germany

Received April 24, accepted July 2, 1987

Summary. NLTE calculations of approximately 200 Fe I and Fe II spectral lines with a comprehensive model atom are presented for a quiet sun model and a grid of fluxtube models. These calculations are compared with LTE results and the departures from LTE in fluxtubes are estimated. For all the fluxtube models tested, the departures from LTE ionization for the Fe I lines are found to be larger than for the quiet sun. Fe II lines show almost no difference between LTE and NLTE. The influence of temperature gradients on the departures is also studied and discussed. The profiles of five Fe I and one Fe II lines are analysed in detail and the errors in empirically determined velocities and temperatures in fluxtubes, introduced by the assumption of LTE, are estimated. It is found that assuming LTE has practically no effect on the determined velocities, but that it may lead to an overestimation of the temperature in fluxtubes at the heights at which the lines are formed.

Key words: radiative transfer – NLTE – solar magnetic fields – fluxtubes – Fe I – Fe II

1. Introduction

Most of the work on the photospheric layers of solar magnetic fluxtubes involving radiative transfer in spectral lines has been restricted to LTE, and only a limited number of NLTE calculations have been carried out. Early studies of NLTE radiative transfer in magnetic regions focussed on the influence of scattering on line formation in a magnetic field. Thus the radiative transfer equations for the Stokes parameters were first formulated and formally solved by Rachkovsky (1963) assuming a two level atom in a homogeneous magnetic field and a Milne-Eddington model atmosphere. Rees (1969) and Domke and Staude (1973) gave numerical solutions for a two level atom with complete redistribution, a homogeneous magnetic field and a Milne-Eddington atmosphere. Domke and Staude included anomalous dispersion in their calculations and also compared the NLTE line profiles with LTE calculations.

Subsequent investigations concentrated on the effects of fluxtube geometry. Stenholm and Stenflo (1977) studied the influence of hot fluxtube walls in 2-D geometry on line profiles, by assuming that the atmosphere inside the fluxtube is simply the quiet sun atmosphere shifted downwards by some value corresponding to the Wilson depression. For a two level atom they found a weakening of the Fe I 5250.2 Å line ranging from a couple of percent to almost 50%, depending on the radius of the fluxtube and on their parameter Q, a nominal collisional excitation cross-section. However, due to the lack of a realistic model atom, Q remained a free parameter in their calculations. Stenholm and Stenflo (1978) extended this analysis to include polarized radiation and Zeeman splitting, but they retained the simple two level atom and fluxtube model.

Finally, Owocki and Auer (1980) have used the Mihalas et al. (1978) code to compare the wings of the Ca K and Mg k lines calculated using 1-D, 1.5-D, and 2-D radiative transfer in a horizontally inhomogeneous atmosphere (representing a periodic arrangement of fluxtubes). They conclude that 1-D is often a usable approximation for spatially averaged profiles, and 1.5-D usually provides an excellent approximation to the full 2-D radiative transfer.

The previous investigations have therefore either been restricted to very idealized situations, or have concentrated on the study of multi-dimensional effects. It is our aim in this paper to estimate the magnitude of NLTE effects and their influence on the line profiles of photospheric lines with a realistic model atom and in a fluxtube atmosphere which is compatible with observational data. Two major restrictions apply to these calculations, namely, the effect of the magnetic field on the line profile is neglected, and the calculations are one-dimensional. The present paper is therefore complementary in nature to the previous studies of NLTE in fluxtubes.

Rees (1969) and Stenholm and Stenflo (1978) have shown that the level populations and line profiles calculated by taking the magnetic field into account explicitly are very similar to approximate results based on assuming zero magnetic fields for the calculation of the level populations or the source function. Therefore, the first restriction should not significantly affect our results, specially since these are based mainly on a comparison of NLTE to LTE line profiles. However, the true shape of the individual line profiles inside fluxtubes will be somewhat different from the ones we calculate due to our neglect of Zeeman splitting. Regarding the second simplification Stenholm and Stenflo (1977, 1978) find that under certain conditions the effects of the fluxtube geometry on the line profiles need not be negligible, but the inclusion of such effects is beyond the scope of the present paper.

The lines of Fe I and II are of particular interest since iron has a rich spectrum. Most magnetograph and related observations of

Send offprint requests to: W. Steenbock

* Present address: Institut für Astronomie und Astrophysik der Universität München, Scheinerstrasse 1, D-8000 München, Federal Republic of Germany

small scale magnetic features have been carried out with Fe I lines, and recent investigations have used large samples of Fe I and II lines to empirically determine the temperature, magnetic field, and velocity structure of fluxtubes (e.g. Solanki and Stenflo, 1984, 1985; Solanki, 1986). We shall therefore present results of NLTE radiative transfer calculations of Fe I and II lines carried out with one of the most comprehensive models of an iron atom currently available, including the effects of inelastic collisions with neutral hydrogen atoms and an improved approximation of the UV radiation field. These calculations are carried out in a number of model atmospheres including two models which reproduce extensive data sets of Fe I and II Stokes I and V spectra obtained in active region plages and the enhanced network. All previous multilevel NLTE calculations of solar Fe I and II lines have been restricted to the quiet sun (e.g. Athay and Lites, 1972; Lites, 1973; Cram et al., 1980; Steenbock, 1985; Watanabe and Steenbock, 1986).

2. Description of the code and the model atom

In order to solve the statistical equilibrium equations simultaneously with the NLTE radiative transfer in lines, we have used the code of Steenbock and Holweger (1984), which has been derived from the code of Auer et al. (1972). The original formulation of the complete linearization method has been replaced by the efficient scheme proposed by Auer and Heasley (1976) following Rybicki (1971). Many modifications have been made to improve its numerical efficiency and to adapt its input physics to cool stars and the special case of iron.

The iron model atom is an extended version of that used by Steenbock (1985) to study NLTE effects in the Sun and the red giant Pollux. For a Grotrian diagram and further details see Gigas (1986) and Watanabe and Steenbock (1986). The model atom consists of 79 Fe I and 20 Fe II levels as well as the Fe III continuum. The levels are interconnected by 52 Fe I and 23 Fe II transitions. For the line absorption coefficient Voigt profiles are used, approximated by up to 30 frequency points per half-profile to account for the important far wings of strong resonance lines. Each term of the model atom is coupled to its parent term in the next ionization stage by photoionization and collision (electron and neutral hydrogen) rates. The photoionization and recombination rates are calculated by solving the appropriate rate-integral using the LTE radiation field J_ν. Because of their importance, not only continuous but also line opacities are taken into account when computing J_ν. Following the scheme worked out by Kurucz (1979) for his ATLAS6-code, wavelength-averaged J_ν values were computed for typically 25 Å wide intervalls using the line opacity distribution function of Kurucz (1979). In the course of NLTE line formation calculations the rate-integrals were held fixed. In adopting this procedure we neglected the change in J_ν at the iron continua caused by the iron continua themselves and the iron lines contained in the line opacities. Owing to the optically thin iron continua and to the broad-band characteristic of the photoionization rate-integrals these approximations should be feasible.

In addition all terms of a given ionization stage are coupled by collision rates. 47 Fe I and 5 Fe II levels are assumed to be purely collisionally coupled to the rest. The temperature dependence of the electron collision rates is estimated with the help of the semi-empirical formulae of Drawin (1966). Collisional cross-sections for allowed Fe I transitions are calculated on the basis of the dipole-approximation. In all other cases πa_0^2 (where a_0 is the Bohr radius) is used. Since there are strong indications that neutral particle collisions are important (Steenbock and Holweger, 1984; Watanabe and Steenbock, 1986) we include collisions with neutral hydrogen by adopting the formulae of Drawin (1968, 1969) and Steenbock and Holweger (1984). It should be noted that these formula are only order of magnitude estimates of the strength of neutral hydrogen collisions. In view of this, a factor has been introduced to scale the collision-strength of Drawin (1968, 1969) and Steenbock and Holweger (1984). As suggested by unpublished work carried out by one of us (Steenbock), a factor of 1/3 has been used.

After calculating the iron level populations, detailed line formation calculations have been performed using the program LINFOR developed in Kiel and modified to accept NLTE departure coefficients. Voigt functions are used to represent the profiles of the line absorption coefficients. Radiation damping has been calculated from inverse lifetimes compiled from several experimental sources. We also include van der Waals damping using mean square radii calculated by Hofsäss (1975) and Unsöld's (1968) classical formula. The van der Waals interaction constant has been modified as proposed by Simmons and Blackwell (1982).

3. Model atmospheres and computational procedure

The NLTE calculations presented here have been carried out in a total of eight model atmospheres. One of these is a modified version of the HSRASP (Chapman, 1979), which is itself a combination of the HSRA (Gingerich et al., 1971) with the convection zone model of Spruit (1974). The chromospheric temperature rise present in the original HSRASP has been replaced by a $T(\tau)$ that runs approximately parallel to the temperature of the Holweger and Müller (1974) model for $\log\tau < -4$. This modification has been carried out in order to get comparable results for the quiet sun and the fluxtube models. As a consequence the source functions of the strongest Fe I lines, for which the outer parts of the atmosphere are more important, do not reflect the chromospheric temperature rise.

Of the remaining seven models, four represent a test grid of fluxtube models (labeled A, B, C, D) and the rest are based on an analysis of polarized spectra (Netw1, Netw2, and Plage). $T(\tau)$ of all eight models is shown in Fig. 1. The seven fluxtube models have all been constructed assuming hydrostatic equilibrium and the thin fluxtube approximation, i.e. they are one dimensional models and magnetic tension has been neglected. Its effects are expected to be relatively small anyway (cf. Pneuman et al., 1986). The electron pressure and the continuum absorption coefficient are calculated with the LTE code described by Gustafsson (1973). Models A, B, and C only differ below $\log\tau = -1$ and run approximately parallel to the modified HSRASP above this depth, while model D has a $T(\tau)$ which is 800 K hotter than model A everywhere. Models A, B, and C serve to test the influence of the temperature near the level where the visible continuum is formed on the magnitude of the NLTE effects. Model D is used to check if any differences in the departures from LTE ionizations found between models A, B, and C are due to the absolute value of the temperature at $\log\tau = 0$, and therefore the intensity of the continuum radiation field, or if it is an effect of the $T(\tau)$ gradient. Lines calculated in LTE with models Netw1 and Netw2 reproduce Stokes V data obtained in the quiet network, while model Plage reproduces data obtained in an active region plage (Solanki, 1986). Since the Fe I and II lines in the visible are (in LTE) relatively insensitive to the temperature structure

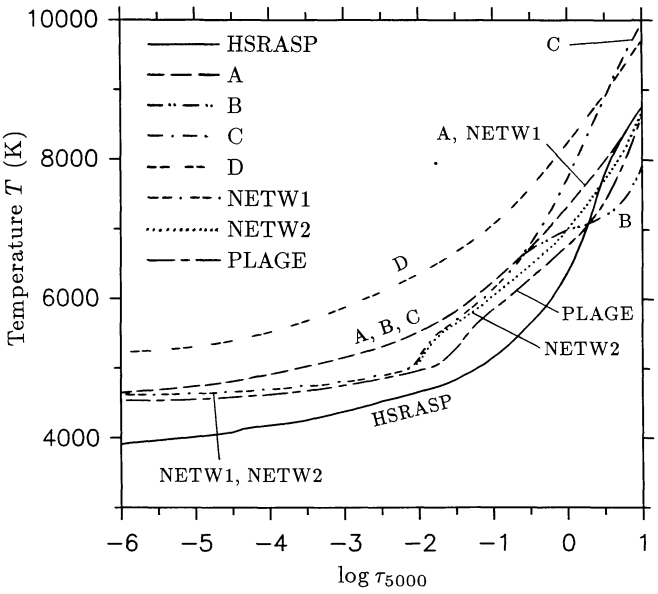

Fig. 1. Temperature T(K) vs. logarithmic optical depth $\log \tau_{5000}$ for a quiet sun model, HSRASP, and seven models of fluxtubes. The various models are identified in the figure and discussed in the text

below $\log \tau \approx -1$, Netw 1 and Netw 2, which differ only in their deepest layers (Netw 1 is similar to model A for $\log \tau > -0.5$), reproduce the observed profiles equally well.

One method of fixing the temperature in the fluxtube near the $\log \tau = 0$ level is by comparing the continuum contrast of the models with values observed near disk centre. The continuum contrasts I_c(fluxtube)/I_c(photosphere) = I_c(model)/I_c(HSRASP) of the various models at $\lambda = 5000$ Å and $\mu = \cos\theta = 1.0$ are listed in Table 1. Observed continuum contrasts of magnetic regions are in general considerably lower than these values. Thus Schmahl (1967), Frazier (1971), and Stellmacher and Wiehr (1973) find continuum contrast values in active region plages ranging from 1.01 to 1.02 at disk centre. Muller (1975), with somewhat better spatial resolution finds contrasts closer to 1.05. Finally, Frazier and Stenflo (1978) infer continuum contrasts of up to 1.18 by compensating for their limited spatial resolution through the use of additional information from polarimeter measurements. For a large number of facular points in quiet regions Muller and Keil (1983) find continuum contrasts between 1.3 and 1.5, after attempting to compensate for seeing effects and Koutchmy (1977) actually finds a value of 2.0 for one facular point. The main problems with the interpretation of continuum measurements derive from the small size of the fluxtubes and the limited spatial resolution of the measurements. Therefore, the higher contrast values derived from high spatial resolution observations, or from the correlation between continuum contrast and magnetic flux are probably the more reliable ones. Furthermore, recently Schüssler and Solanki (1987) used an indirect method to derive a lower limit of 1.4 to the continuum contrast. We therefore attempt to take the different measured values into account in the different continuum contrasts of models Netw1 (>lower limit of Schüssler and Solanki, 1987), Netw2 (mean of the values of Muller and Keil, 1983), and Plage (near the value of Frazier and Stenflo, 1978).

In Sect. 4 the effects of NLTE on the equivalent widths of 214 Fe I and II lines are discussed. These lines are not necessarily the same ones as in the model atom although they only connect levels which are also radiatively coupled in the model atom. This means that purely collisionally coupled levels are not used. Disk centre solar equivalent widths of these lines have been taken from various sources (Ruland et al. 1980; Mäckle et al., 1975; Holweger, 1967). When these sources gave different results or when some lines of interest were not present in any of them, equivalent widths were measured from the solar atlas of Delbouille et al. (1973). These lines, along with their $\log gf$ and W_λ values are listed in Table 2. Here gf is the weighted oscillator strength of the line. The elemental abundance by number relative to hydrogen, $\log \varepsilon$, is assumed to be 7.46. This means that in order to consistently reproduce the solar equivalent widths, we had to use oscillator strengths which differ slightly from those measured by Blackwell et al. (1982). The relation between our and their values is: $\log gf = \log gf_{\text{Blackwell}} - 0.039$, except for the lines in multiplet 62 for which $\log gf = \log gf_{\text{Blackwell}} - 0.102$.

The procedure for determining the departures from LTE is as follows. First the $\log gf\varepsilon$ values are determined in LTE by fitting the observed equivalent widths W_λ of the quiet sun line profiles using the HSRASP model. These $\log gf\varepsilon$ values are then used to calculate the LTE W_λ values for the other seven models. Then the lines are recalculated in NLTE, with the $\log gf\varepsilon$ values being varied until the equivalent widths equal the LTE values for the respective models. This process is carried out for each model individually. $\Delta \log \varepsilon = \log gf\varepsilon_{\text{NLTE}} - \log gf\varepsilon_{\text{LTE}}$, the difference in elemental abundance between LTE and NLTE fits of the equivalent widths, is then used as a measure of the strength of NLTE effects. This procedure has been previously used by e.g. Steenbock and Holweger (1984), and Steenbock (1985). It is a good measure of the departures from LTE studied here, since these are mainly due to overionization of Fe I into Fe II (i.e. Fe I NLTE is mostly an opacity effect and not a source function effect). For this reason we also wish to note that what we term NLTE effects in the following should more precisely be called effects of NLTE ionization.

In addition to these equivalent width results we also present the full line profiles of a small sample of spectral lines in order to estimate how strongly NLTE affects the shape of the line profile, and how it may influence empirically determined fluxtube properties. The six lines for which the full line profiles have been analysed are listed in Table 3. They have been chosen to represent lines with a range of excitation potentials and equivalent widths. They also include Fe I 5250.2 Å and 6173.3 Å, two lines often used for magnetograph observations and fluxtube diagnostics.

Throughout the following line profile calculations using the appropriate level-populations, the microturbulence velocity for the disc center is chosen to be 1.0 km s^{-1}. When computing NLTE-level populations a microturbulence velocity for the integrated disk of 1.35 km s^{-1} is assumed. The latter value is uncritical for the result. In the following τ always denotes τ(5000 Å).

Table 1. Disk centre continuum contrasts I_c(model)/I_c(HSRASP) at $\lambda = 5000$ Å

Model atmospheres:	HSRASP	A	B	C	D	Netw1	Netw2	Plage
Continuum contrasts:	1.00	1.63	1.36	1.99	2.50	1.58	1.40	1.20

Table 2a. Fe I lines

λ	Multiplet number	χ_e	log(gf)	W_λ
5127.684	1	0.05	−6.164	14.3
5225.534	1	0.11	−4.700	68.0
5247.059	1	0.09	−4.985	66.0
5250.217	1	0.12	−4.977	65.0
4389.251	2	0.05	−4.577	74.0
4445.476	2	0.09	−5.480	36.0
4489.745	2	0.12	−4.005	92.0
8075.153	12	0.91	−4.913	32.0
8204.090	12	0.91	−5.751	6.5
6221.643	13	0.86	−6.207	2.0
6280.624	13	0.86	−4.426	62.0
6353.687	13	0.86	−3.826	81.0
6353.849	13	0.91	−6.295	1.5
6498.945	13	0.96	−4.738	43.0
6574.254	13	0.99	−4.885	25.0
6648.121	13	1.01	−5.657	5.2
5956.706	14	0.86	−4.433	51.0
6120.249	14	0.91	−5.840	4.0
5405.748	15	0.99	−1.883	213.0
5434.534	15	1.01	−2.162	163.0
5501.477	15	0.96	−2.916	110.0
5506.786	15	0.99	−2.836	123.0
4939.693	16	0.86	−3.379	96.0
4994.136	16	0.91	−3.119	105.0
5079.746	16	0.99	−3.259	97.0
5083.345	16	0.96	−2.997	111.0
5127.365	16	0.91	−3.346	98.0
7180.004	33	1.48	−4.686	16.0
6710.323	34	1.48	−4.763	13.0
6739.524	34	1.56	−4.815	10.0
6801.849	34	1.61	−5.666	1.4
6851.652	34	1.61	−5.200	4.0
5853.161	35	1.48	−5.077	6.0
4733.597	38	1.48	−3.026	84.0
4602.003	39	1.61	−3.051	71.0
4602.947	39	1.48	−2.259	119.0
8327.061	60	2.20	−1.483	173.0
8387.782	60	2.18	−1.456	179.0
8514.082	60	2.20	−2.110	120.0
8824.200	60	2.19	−1.445	187.0
6136.999	62	2.20	−3.052	63.0
6151.623	62	2.18	−3.256	46.0
6173.341	62	2.22	−2.816	67.0
6213.437	62	2.22	−2.569	79.0
6219.287	62	2.20	−2.417	87.0
6265.141	62	2.18	−2.513	84.0
6297.799	62	2.22	−2.693	73.0
6335.337	62	2.20	−2.212	100.0
6430.856	62	2.18	−1.952	117.0
6015.253	63	2.22	−4.473	4.8
6082.718	64	2.22	−3.578	28.0
6240.653	64	2.22	−3.256	44.0
5198.717	66	2.22	−2.174	95.0
8804.600	106	2.27	−3.167	58.0
6392.538	109	2.28	−3.857	16.0
6481.878	109	2.28	−2.860	63.0
6861.945	109	2.42	−3.718	17.0
6911.522	109	2.42	−3.900	12.0
7151.404	109	2.48	−3.538	22.0
6663.450	111	2.42	−2.518	81.0
6750.164	111	2.42	−2.450	77.0
6945.210	111	2.42	−2.358	82.0
6978.862	111	2.48	−2.376	79.0
5322.049	112	2.28	−2.778	61.0
5253.033	113	2.28	−3.749	17.0
5678.609	113	2.42	−4.780	1.5
5141.746	114	2.42	−2.012	91.0
4794.359	115	2.42	−3.803	11.0
6988.533	167	2.40	−3.379	32.0
6393.612	168	2.43	−1.458	139.0
6494.994	168	2.40	−1.292	160.0
6593.884	168	2.43	−2.250	87.0
6667.445	168	2.45	−4.271	5.0
6136.624	169	2.45	−1.386	141.0
6191.571	169	2.43	−1.428	140.0
6252.565	169	2.40	−1.593	127.0
5916.257	170	2.45	−2.840	53.0
7461.527	204	2.56	−3.383	26.0
6746.975	205	2.61	−4.259	3.7
6839.835	205	2.56	−3.278	29.0
6860.327	205	2.61	−4.044	6.0
7069.540	205	2.56	−4.325	3.7
6475.632	206	2.56	−2.769	54.0
6609.118	206	2.56	−2.590	64.0
6783.280	206	2.56	−4.468	2.6
6065.494	207	2.61	−1.563	117.0
6137.701	207	2.59	−1.442	139.0
6200.321	207	2.61	−2.309	74.0
6322.694	207	2.59	−2.323	75.0
6139.651	208	2.59	−4.563	1.8
6199.508	208	2.56	−5.249	0.4
6290.532	208	2.59	−4.531	2.0
5701.557	209	2.56	−2.084	86.0
5778.463	209	2.59	−3.400	20.0
7540.444	266	2.73	−3.830	8.0
7114.574	267	2.69	−3.846	8.0
7228.700	267	2.76	−3.198	25.0
7261.016	267	2.73	−3.441	17.0
6703.576	268	2.76	−2.952	35.0
6806.856	268	2.73	−3.070	31.0
6180.209	269	2.73	−2.626	52.0
5044.218	318	2.85	−1.979	75.0
5068.771	383	2.94	−1.113	136.0
5232.952	383	2.94	−0.124	351.0
8515.122	401	3.02	−2.027	84.0
8582.271	401	2.99	−2.177	76.0
8621.618	401	2.95	−2.269	73.0
8747.438	401	3.02	−3.261	17.0
7583.796	402	3.02	−1.847	89.0
7748.284	402	2.95	−1.721	103.0
6971.917	404	3.02	−3.325	12.0
7112.170	404	2.99	−2.862	30.0
5807.792	552	3.29	−3.261	7.0
5827.884	552	3.28	−3.164	8.8
5217.396	553	3.21	−1.100	122.0
5253.468	553	3.28	−1.575	81.0
6145.411	685	3.37	−3.727	2.2
6271.283	685	3.33	−2.707	21.0
5569.631	686	3.42	−0.482	185.0
5576.099	686	3.43	−0.843	135.0
5784.366	686	3.40	−2.510	25.0
4907.735	687	3.43	−1.650	65.0
4946.395	687	3.37	−1.124	103.0
4950.111	687	3.42	−1.486	76.0
6246.327	816	3.60	−0.844	127.0
6301.508	816	3.65	−0.761	132.0
6336.830	816	3.69	−0.859	119.0
6411.658	816	3.65	−0.635	143.0
8652.475	1050	4.15	−2.592	7.3
6880.637	1051	4.15	−2.298	11.0
6999.885	1051	4.10	−1.344	57.0
7022.957	1051	4.19	−1.048	72.0
7038.220	1051	4.22	−1.172	62.0
7090.390	1051	4.23	−1.066	69.0
7130.925	1051	4.22	−0.724	95.0
6653.911	1052	4.15	−2.323	10.0
6704.500	1052	4.22	−2.501	6.0
6725.364	1052	4.10	−2.118	17.0
6786.860	1052	4.19	−1.827	25.0
6916.686	1052	4.15	−1.245	61.0
5677.695	1057	4.10	−2.565	6.0
5473.910	1062	4.15	−0.746	85.0
5525.552	1062	4.23	−1.095	58.0
5543.944	1062	4.22	−1.033	62.0
7306.570	1077	4.18	−1.514	43.0
7411.162	1077	4.28	−0.433	120.0
7491.652	1077	4.30	−0.983	72.0
7511.031	1077	4.18	0.035	200.0
7710.367	1077	4.22	−1.101	70.0
6898.307	1078	4.22	−2.114	14.0
7007.976	1078	4.18	−1.761	29.0
5638.271	1087	4.22	−0.754	81.0
5641.448	1087	4.26	−0.968	64.0
5705.473	1087	4.30	−1.375	39.0
5775.083	1087	4.22	−1.122	58.0
5522.454	1108	4.21	−1.353	44.0
5608.981	1108	4.21	−2.218	10.0
5652.327	1108	4.26	−1.717	24.0
5661.354	1108	4.28	−1.807	20.0
7937.150	1136	4.31	−0.024	175.0
7998.953	1136	4.37	0.014	174.0
8046.058	1136	4.41	−0.139	147.0
8220.388	1136	4.32	0.155	215.0
8248.137	1136	4.37	−1.055	67.0
7507.237	1137	4.41	−0.995	64.0
7531.153	1137	4.37	−0.617	95.0
7586.027	1137	4.31	−0.257	138.0
6034.038	1142	4.31	−2.315	7.0
6054.075	1142	4.37	−2.260	7.0
8598.836	1153	4.39	−1.221	56.0
8610.609	1153	4.43	−1.732	24.0
7780.568	1154	4.47	−0.143	137.0
7832.208	1154	4.43	−0.027	157.0
6733.153	1195	4.64	−1.379	26.0
6828.596	1195	4.64	−0.816	58.0
6855.166	1195	4.56	−0.630	76.0
8526.676	1270	4.91	−0.622	64.0
8527.847	1270	5.02	−1.575	11.0
8784.400	1270	4.93	−1.231	26.0

Table 2b. Fe II lines

λ	Multiplet number	χ_e	$\log(gf)$	W_λ
5000.735	25	2.78	−4.486	11.0
5132.674	35	2.81	−3.996	25.0
5136.800	35	2.84	−4.351	13.0
5154.412	35	2.84	−3.867	29.0
4993.352	36	2.81	−3.640	40.0
4491.408	37	2.85	−2.794	74.0
4508.289	38	2.85	−2.603	84.0
4576.339	38	2.84	−3.087	62.0
4620.520	38	2.83	−3.346	51.0
6369.463	40	2.89	−4.114	20.0
6432.683	40	2.89	−3.575	42.0
6516.083	40	2.89	−3.266	56.0
5256.933	41	2.89	−4.098	19.0
5284.112	41	2.89	−3.072	61.0
4923.930	42	2.89	−1.682	165.0
5991.378	46	3.15	−3.476	35.0
6084.105	46	3.20	−3.732	23.0
6113.329	46	3.22	−4.084	12.0
6141.010	46	3.22	−4.679	3.5
5264.808	48	3.23	−3.079	49.0
5414.075	48	3.22	−3.589	27.0
5197.576	49	3.23	−2.461	79.0
5234.630	49	3.22	−2.271	90.0
5325.560	49	3.22	−3.216	43.0
5425.259	49	3.20	−3.219	44.0
7301.577	72	3.89	−3.663	9.0
7479.701	72	3.89	−3.616	10.0
7222.397	73	3.89	−3.204	21.0
7224.464	73	3.89	−3.204	21.0
7310.201	73	3.89	−3.237	20.0
7711.731	73	3.90	−2.631	47.0
6149.249	74	3.89	−2.705	40.0
6247.562	74	3.89	−2.340	58.0
6416.928	74	3.89	−2.678	42.0
6456.391	74	3.90	−2.189	66.0

4. Influence of departures from LTE on the equivalent widths

In Fig. 2 $\Delta\log\varepsilon = \log gf\varepsilon_{\mathrm{NLTE}} - \log gf\varepsilon_{\mathrm{LTE}}$ is plotted vs. W_λ for the modified HSRASP. Dots represent Fe I lines with excitation potential of the lower level $\chi_e \leqq 3.5$ eV, circles Fe I lines with $\chi_e > 3.5$ eV, and crosses Fe II lines. The apparent division of the Fe I lines into two or more distinct groups is only a line selection effect. Especially for lines with $W_\lambda < 100$ mÅ (in the quiet sun) the departures in level population from LTE at a fixed depth are the same for all levels, resulting from a general over-ionization of Fe I. As pointed out by Steenbock (1985) the dependence of $\Delta\log\varepsilon$ on excitation potential reflects the different heights of formation and shows the depth dependence of the LTE departures, which approach zero near the continuum forming layer.

In Fig. 3 $\Delta\log\varepsilon$ is plotted vs. W_λ for the models HSRASP, A, B, C, D, and Netw1. The smoothed mean curves for Fe I lines with $\chi_e \leqq 3.5$ eV are shown in Fig. 3a, while those for the Fe I lines with $\chi_e > 3.5$ eV are shown in Fig. 3b. The W_λ scale has been chosen such that curves resulting from the fluxtube model atmospheres fill the frame. This means that for the HSRASP only the lines with $W_\lambda \leqq 140$ mÅ are visible in this figure. The results for the various atmosphere models are marked in the same manner as in Fig. 1. The low excitation Fe I lines are concentrated into two more or less distinct groups (Fig. 3a), which are represented by separate curves for each model atmosphere. The curves marked "a" represent most of the lines, while the curves marked "b" are smoothed means of $\Delta\log\varepsilon$ vs. W_λ of a few weaker lines with low χ_e. These lines have relatively high formation levels and thus a larger sensitivity to ionization departures. This distinction into two groups does not have a deeper physical significance, but is rather a line selection effect caused by a scarcity of unblended lines lying in the intermediate range. The two curves may, therefore, be considered as showing the extremes which $\Delta\log\varepsilon$ can take for the low χ_e Fe I lines of a given model. In Fig. 3b a more or less distinct group of lines with large W_λ show consistently smaller (and sometimes negative) values of $\Delta\log\varepsilon$, as compared to the rest of the lines. These with anomalous $\Delta\log\varepsilon$ have highly excited upper levels which however are always radiative coupled in the model atom. These levels possibly are not treated properly in our model atom (incomplete model atom), and may therefore show wrong $\Delta\log\varepsilon$ values. The calculated $\Delta\log\varepsilon$ of these lines are not compatible with values measured in red giants (Steenbock, unpublished result). In order to avoid confusion we have plotted them on a separate curve labelled "b".

Fe II lines have not been plotted, since their $\Delta\log\varepsilon$ values are of the order of those for the HSRASP or even smaller, so that for these lines LTE seems to be an excellent approximation, for all the models tested. A more definite statement can only be made after Fe II has been modelled and calculated in greater detail, as has been

Table 3. Lines selected for full profile analysis

Ion	Wavelength	Multiplet number	χ_e (eV)	Transition	W_λ (mÅ)
Fe I	5083.3450	16	0.96	$a\,^5F_3 - z\,^5F^o_3$	107
Fe II	5197.5742	49	3.23	$a\,^4G_{2\frac{1}{2}} - z\,^4F^o_{1\frac{1}{2}}$	79
Fe I	5232.9493	383	2.94	$z\,^7P^o_4 - e\,^7D_5$	351
Fe I	5250.2171	1	0.12	$a\,^5D_0 - z\,D^o_1$	70
Fe I	5638.2675	1087	4.22	$y\,^5F^o_4 - g\,^5D_3$	81
Fe I	6173.3433	62	2.22	$a\,^5P_1 - y\,^5D^o_0$	67

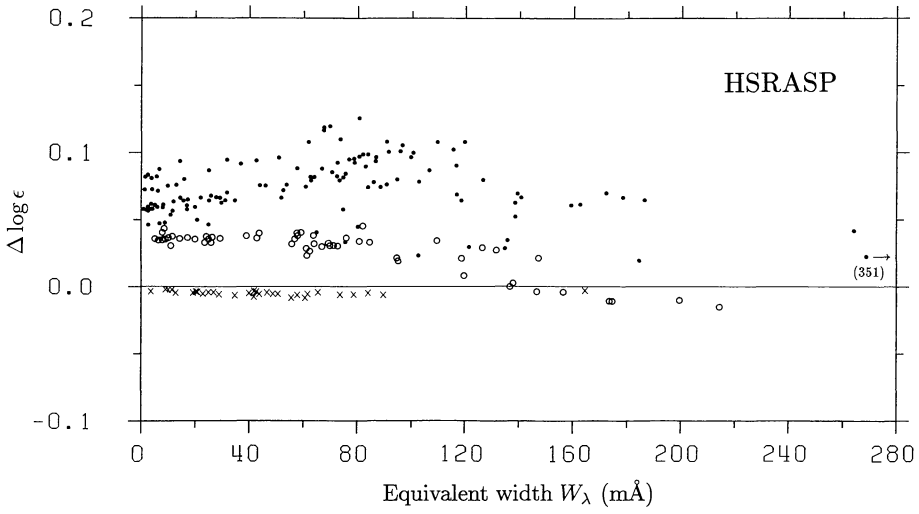

Fig. 2. $\Delta \log \varepsilon = \log gf\varepsilon_{\mathrm{NLTE}} - \log gf\varepsilon_{\mathrm{LTE}}$ vs. the equivalent width W_λ for lines calculated with quiet sun model HSRASP, where ε is the abundance and gf is the weighted oscillator strength. Dots represent Fe I lines with $\chi_e \leqq 3.5$ eV, open circles Fe I lines with $\chi_e > 3.5$ eV, crosses Fe II lines. The point with the arrow near the right boundary lies outside the frame. Its equivalent width is indicated in brackets

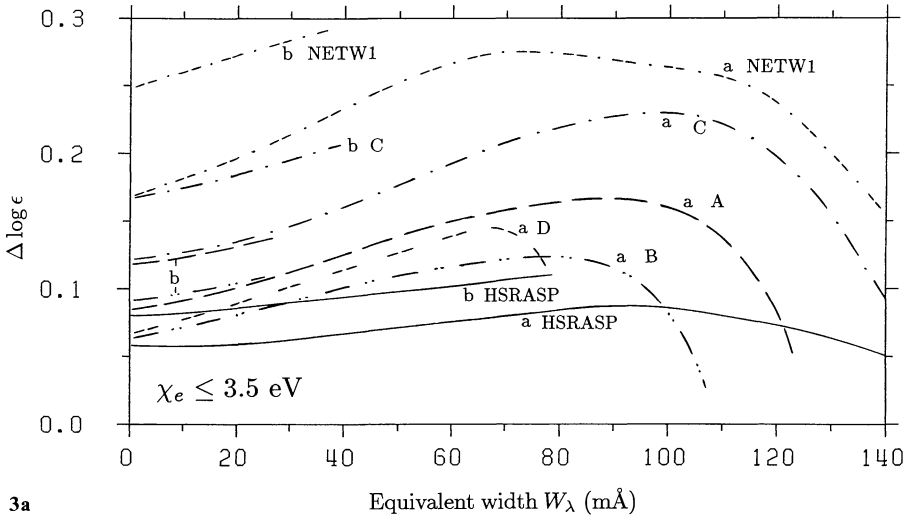

3a

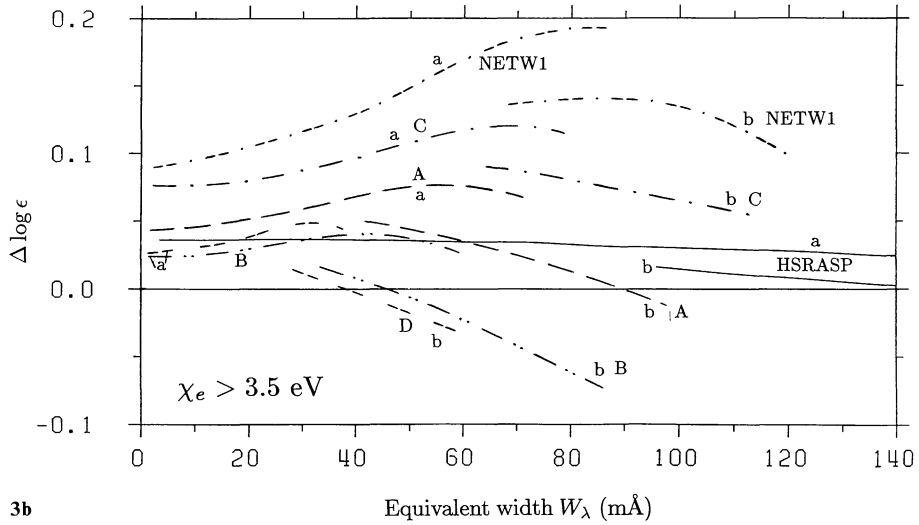

3b

Fig. 3a and b.
$\Delta \log \varepsilon = \log gf\varepsilon_{\mathrm{NLTE}} - \log gf\varepsilon_{\mathrm{LTE}}$ vs. W_λ for lines calculated with the models HSRASP, A, B, C, D, and Netw1. The results for the different models are represented by the same symbols as in Fig. 1. For most of the curves the models are directly identified. The curves marked "a" represent most of the lines, while curves labelled "b" refer to smaller groups of lines discussed in the text. **a.** Fe I lines with $\chi_e \leqq 3.5$ eV. The "b" curve of model D lies very close to the "b" curve of model B and has not been plotted **b.** Fe I lines with $\chi_e > 3.5$ eV

done by Watanabe and Steenbock (1986). As demonstrated by a comparison of Fig. 3a with Fig. 3b, the trend towards decreasing $\Delta \log \varepsilon$ with increasing χ_e persists also for our grid of test models. It is qualitatively affected neither by the absolute temperature of the atmosphere (compare models A and D), nor by the difference in temperature between the levels where the continuum and the lines are formed (compare models A, B, and C). A certain dependence of $\Delta \log \varepsilon$ on W_λ is also observed, which has a similar form for all the models as well. The *absolute values* of $\Delta \log \varepsilon$, on the other hand, are seen to vary considerably from model to model, with the quiet sun model HSRASP showing the smallest departures. In the following we shall attempt a crude explanation of these variations. More details on the NLTE mechanisms in Fe I/II are to be found in e.g. the review by Rutten (1987).

The value of $\Delta \log \varepsilon$ is fixed by the ratio of the NLTE level populations N_i to the LTE level populations N_i^*, i.e. by the departure coefficients $b_i = N_i/N_i^*$. Departure coefficients as a function of height for a quiet sun atmosphere (Holweger and Müller, 1974) have been plotted by Steenbock (1985). Of particular importance are the b_i values in the depth range in which the equivalent widths of the lines are formed ($-3 \lesssim \log \tau \lesssim -1$). If we neglect collisions for the moment, then the N_i in this layer are determined almost exclusively by photo-ionization and recombination; i.e. departures from thermal excitation due to radiative transfer in the spectral lines play only a minor role. The departure coefficients are therefore determined by the difference between the ionizing UV continuum radiation field J_ν and the local Planck function B_ν. The radiation temperature of J_ν at the line formation region can be approximated by $T_e(\log \tau \approx 0)$ and that of B_ν by $T_e(\log \tau \approx -2)$, so that the departures are functions of the temperature gradient. Since only ionization departures are present $\Delta \log \varepsilon$ with fixed W_λ is approximately proportional to $-\log b_i(\log \tau \approx -2)$ of the lower level. See also Athay and Lites (1972) for a discussion.

This dependence is clearly visible when we compare the curves of models A, B, and C in Fig. 3. These models are practically identical at the height at which the lines are formed, differing only in the layers at which the continuum is produced. The higher the temperature near $\log \tau = 0$ the larger are the departures from LTE. Model *D*, which is hotter than model A throughout, but has a similar temperature gradient, shows lower $\Delta \log \varepsilon$, mainly due to the reduced height of formation of the lines caused by the higher temperature. Therefore, the lines are formed at a depth where the inbalance between J_ν and B_ν is smaller. As a result the departure from LTE for a particular line in model D is generally smaller than for the same line in model A.

The large departures shown by model Netw1 can also be explained by the difference in temperature gradient compared to model A, but now mainly in the line formation region around $\log \tau \approx -2$. From the above results we conclude that the temperature gradient is one of the main parameters influencing the extent of the departures from LTE.

The initial increase of $\Delta \log \varepsilon$ as a function of W_λ is a consequence of the increasing height of formation of the lines, and of the increasing values of the departure coefficients with height. The decrease in $\Delta \log \varepsilon$ for the strongest lines results from their saturation: their equivalent widths are determined mainly by their strong wings formed deeper in the atmosphere where the departure coefficients approach unity. However, as will be seen in the next section, the strongest lines show the largest effects of NLTE on their profile *shapes*.

In Fig. 4 the $\Delta \log \varepsilon$ values of the individual lines are plotted for the models Netw2 and Plage. Since these two models reproduce extensive polarimetric and continuum contrast observations relatively well at disk centre, the $\Delta \log \varepsilon$ values shown in Fig. 4 may be regarded as estimates of the true departures from LTE inside small solar magnetic fluxtubes. The behaviour of $\Delta \log \varepsilon$ for the two models is consistent with the discussion of the other models.

A comparison of Fig. 4 with Fig. 2, shows clearly that departures from LTE are considerably larger in fluxtubes than in the quiet photosphere. It is also of considerable interest to note that the departures for low χ_e Fe I lines are particularly large, since these lines also have the strongest observed weakenings in fluxtubes (e.g. Solanki and Stenflo, 1984, 1985). Since these lines are the most temperature sensitive as well, the NLTE line weakenings mimic the line weakening induced by an increase in temperature. This is not surprising, since the temperature weakening, like the decrease in W_λ due to departures from LTE, is to a large part a result of the ionization of Fe I into Fe II. Departures from LTE ionization will therefore have a significant effect on the empirically determined LTE temperature of, and perhaps also the velocities in, fluxtubes. However, in order to obtain a better estimate of the effects of NLTE on these quantities, we have to consider the influence of NLTE on the complete line profile, since the temperature and velocity are often determined from the line depths and widths. This is done in the next section.

5. Influence of departures from LTE on line profiles

Recently the velocity amplitude inside magnetic fluxtubes has been determined from the widths of integrated Stokes *V* profiles (which are good approximations of the *I* profiles inside fluxtubes in the absence of Zeeman splitting) of Fe I and II lines with the help of LTE model calculations (Solanki, 1986). To test the reliability of velocities determined in this manner it is therefore necessary to compare the shapes of line profiles calculated in NLTE with those calculated in LTE. We do this for the six lines in Table 3 by choosing $\log gf\varepsilon$ for the NLTE profiles such that they have the same W_λ as the corresponding LTE profiles for all the models (the procedure is similar to the one described in Sect. 3). By plotting the two profiles together any difference in profile shape becomes clearly visible. By requiring the NLTE profiles to have the same W_λ as their LTE counterparts, we are indirectly fitting them to the observed line profiles for models HSRASP, Netw1, Netw2, and Plage, since the LTE line profiles calculated with these models have equivalent widths very similar to those of the observed profiles in the quiet sun (HSRASP) and in fluxtubes (Netw1, Netw2, Plage). The LTE (solid) and NLTE (dashed) half-profiles of the six lines listed in Table 3 are shown in Fig. 5 for $W_\lambda(\text{NLTE}) = W_\lambda$ (LTE). Each line is plotted for the models HSRASP, Netw2, and Plage. The largest change in line shape is shown by the strongest line, Fe I 5232.9 Å, the smallest by the Fe II line at 5197.6 Å. Except for Fe I 5232.9 Å, the difference in half-width between LTE and NLTE profiles is smaller than $100\,\text{m s}^{-1}$ for all the lines in each model. This is negligible when compared to the broadening due to velocity of ~ 1.5–$4\,\text{km s}^{-1}$ found in fluxtubes (Solanki, 1986). The difference for Fe I 5232.9 Å is somewhat larger, being of the order of 200–$500\,\text{m s}^{-1}$. Even this value is small compared to the observed non-thermal, non-magnetic broadening.

The fact that only the difference in width between the I_V and Stokes *I* profiles was used to estimate the velocity amplitudes in fluxtubes, reduces the error in the derived velocities due to departures from LTE even further. Since the change in profile shape of the lines calculated with the fluxtube models and with the

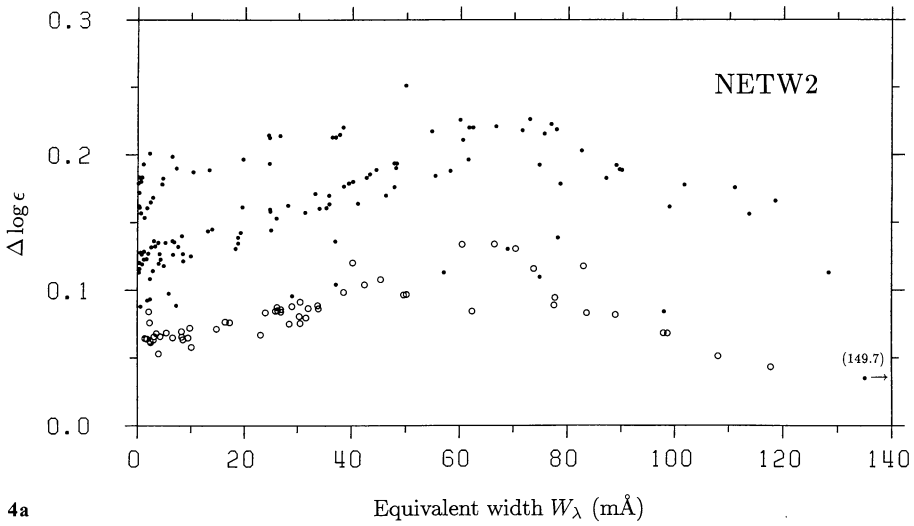

4a

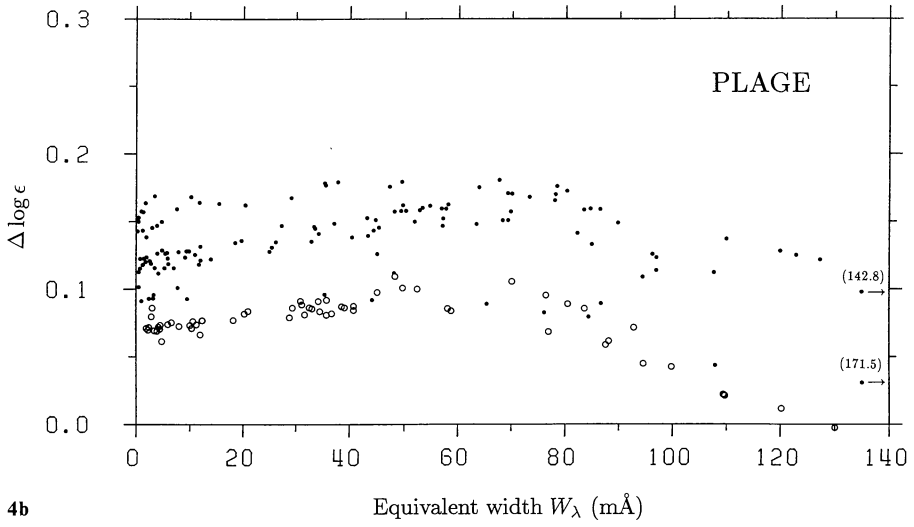

4b

Fig. 4a and b. $\Delta \log \varepsilon = \log gf\varepsilon_{\mathrm{NLTE}} - \log gf\varepsilon_{\mathrm{LTE}}$ vs. W_λ for lines calculated with the models Netw2 and Plage. The symbols are the same as in Fig. 2. Fe II lines have not been plotted, since they all lie very close to zero. Lines with equivalent widths larger than 140 mÅ are indicated by arrows. Their W_λ are given in brackets. **a**. Model Netw2. **b**. Model Plage

quiet sun model are qualitatively similar for all the models (the NLTE profiles are slightly broader for all lines except Fe I 5232.9 Å), the difference in line width between I_V and Stokes I is less changed by NLTE than the line width of either of the two individual profiles. We therefore conclude that the empirical determination of velocities in fluxtubes from line widths is not significantly affected by NLTE effects. We wish to note that Zeeman splitting has not been taken into account for these calculations, so that all the line profiles shown are for magnetic field strength zero, but we do not expect this simplification to affect our conclusion.

To avoid smearing out the differences between the LTE and NLTE line profiles we have not broadened them with any velocity except a microturbulence. This means the line profiles shown in Fig. 5 are too deep and too strongly "U" shaped as compared to the data. Comparisons of the line profile shapes have been carried out for the other models as well. As expected, the largest NLTE induced changes in line shape are shown by the model Netw1, which also exhibited the largest effects of NLTE on the equivalent width (Sect. 4). However, the conclusion that the line width at half minimum is only slightly affected by NLTE for a fixed W_λ remains valid for these models as well.

The differences in line widths are often larger when NLTE profiles are calculated with the same $\log gf\varepsilon$ as the LTE profiles. However, now the NLTE profiles are generally narrower than the LTE profiles. This difference in width is due to the line weakening caused by NLTE overionization, which, for these lines with partly saturated cores, leads to a reduction of the damping wings and consequently of the line widths. Since, in this case, the NLTE line profiles are also weaker than the LTE line profiles, they in general do not provide a good fit to the observed profiles. We, therefore, feel that the calculations which keep W_λ fixed are of greater value for estimating the error in the turbulence velocity derived in LTE.

Next, let us turn to the influence of NLTE on the empirically determined fluxtube temperature. Since the temperature is usually determined from the weakening of spectral lines, this is equivalent to studying the influence of NLTE on the line depth. If we calculate LTE and NLTE profiles using the *same* $\log gf\varepsilon$ values, then the Fe II line at 5197.6 Å is practically unaffected by NLTE, while the low excitation lines Fe I 5250.2 Å and 6173.3 Å show the

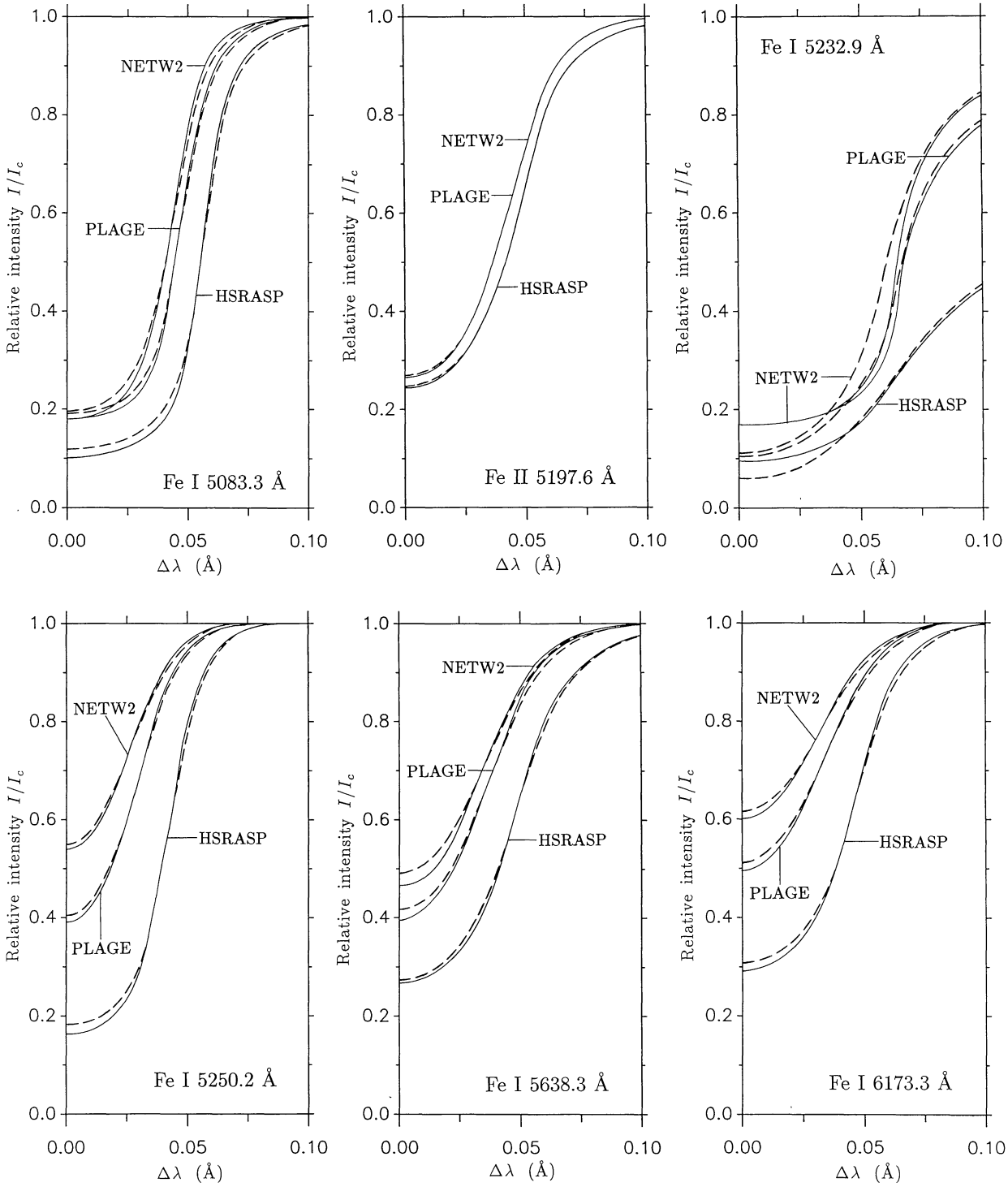

Fig. 5. Line profiles (I/I_c vs. $\Delta\lambda$, the wavelength measured from line centre) of the six lines listed in Table 3 for the models HSRASP, Netw2, and Plage as marked in the figure. The solid curves are LTE profiles, the dashed curves NLTE profiles with $\log gf\varepsilon$ chosen such that W_λ is the same for LTE and NLTE profiles

largest effect. This yet again illustrates how NLTE over-ionization closely simulates the effect of a higher temperature in the fluxtube. In particular the NLTE profiles of model Plage resemble the LTE profiles of model Netw2, suggesting that the true temperature in the fluxtubes of the observed network region lies between those of model Plage and Netw2, and may actually be closer to the temperature of the former. The influence of neglecting departures from LTE on empirically determined model atmosphere temperature structures has been investigated in great detail by Rutten and Kostik (1982) for the quiet Sun. They conclusively demonstrate that the spectrum of Fe I/II can be equally well reproduced in LTE as well as in NLTE. Only, the temperature derived empirically with the two methods will be different. Our calculations suggest that the same is the case for fluxtube atmospheres. Furthermore,

since the departures from LTE are larger inside fluxtubes, the temperature derived in LTE may be wrong by a larger amount. Due to the unavailability of an empirical NLTE model of fluxtubes based on the same observational data as the LTE models, we are unable to carry out an analysis similar in scope to the one of Rutten and Kostik (1982).

6. Summary and conclusions

In this paper we have studied the effects of NLTE on photospheric Fe I and II spectral lines calculated with various model atmospheres, including a model of the quiet sun, a grid of four test models of fluxtubes, and three empirical models of solar magnetic fluxtubes. Departures from LTE are studied as a function of line parameters like excitation potential and equivalent width, and also as a function of the temperature stratification. We have taken the simpler course of using empirical models based on LTE calculations and then estimating the errors resulting from this assumption, instead of the more satisfactory method of determining the model structure by comparing NLTE calculations with the observations. The latter approach is a long term aim, but is beyond the scope of the present investigation.

We find that the errors induced into the abundances by assuming LTE are larger for all the fluxtube models tested, than for the quiet sun model. Maximum errors of the order of a factor of 2 are found for the fluxtube model exhibiting the largest departures from LTE. We demonstrate that the main effect can be crudely explained by changes (from model to model) in the ratio of the electron temperature at the level at which the continuum is formed ($\log\tau \approx 0$) to the electron temperature at the level where the lines are formed ($\log\tau \approx -2$). Since the departures from LTE depend so strongly on the value of $T_e(\log\tau \approx 0)$, it is important to obtain better values of fluxtube temperatures at this depth. The presently available estimates have in general been determined either from direct continuum contrast measurements or from a comparison of fluxtube, average active region and quiet sun line profiles. Both methods have their disadvantages, as is reflected by the large spread of values in the literature. Therefore, it may be better to use infrared observations of Stokes V in the spectral range 1.5–1.7 μ, where the continuum absorption coefficient has a minimum. Since lines in this spectral range are formed close to the level at which the ionizing UV continuum is produced, so that $T_e(\tau_{\text{lines}}) \approx T_e(\tau_{\text{continuum}})$ and consequently ionization departures are small, we expect them to show only minor departures from LTE.

We have also investigated the errors introduced into empirically determined temperatures and velocities in fluxtubes by assuming LTE. Whereas the departures from LTE are found to have only an insignificant effect on the determination of velocities, their effects will have to be taken into account in a proper model of fluxtube temperatures. To estimate the true magnitude of such errors is not simple, since they depend strongly on the assumed fluxtube model. Below we outline an extreme (and probably non-realistic) example of how NLTE effects alone may account completely for the observed line weakenings.

Lines calculated using the proper NLTE ionization are weaker than those calculated assuming LTE ionization by an amount determined roughly by $T_e(\tau_{\text{continuum}})/T_e(\tau_{\text{lines}})$. It would therefore theoretically be possible to reproduce the observed line weakenings in NLTE by keeping the temperature in the fluxtube equal to the temperature of the surroundings (at equal τ) near $\log\tau = -2$ and by increasing it only near $\log\tau = 0$, i.e. by increasing the temperature gradient in the fluxtube. Therefore lines can be weakened without an increase in T at the level at which they are formed. Since in LTE an increase in $T_e(\tau_{\text{lines}})$ is required to reproduce a line weakening, such a model atmosphere would not give rise to any major change in line depth in LTE. Once more, we can only point to the importance of determining the temperature near $\log\tau = 0$ as a means of testing this and similar suggestions.

Finally, we wish to present a suggestion for future work. A natural extension of the present analysis would be to study all four Stokes parameters in NLTE, i.e. to include the effects of a magnetic field. A simple way of doing this would be by following the suggestion of Landi Degl'Innocenti (1976) and using the departure coefficients calculated without a magnetic field in the source function and the absorption matrix of the Unno equations.

Acknowledgements. We are greatly indebted to H. Holweger for initiating this project and for his continuing encouragement. We wish to thank J.O. Stenflo for his support and for critically reading the manuscript. Å. Nordlund kindly provided the continuum opacity code. This is gratefully acknowledged. We also wish to express our gratitude to the referee R. Rutten, whose very detailed comments have been instrumental in improving both our understanding and the presentation. This work was partially supported by grant No. 2.666-0.85 from the Swiss National Science Foundation (S.K.S.) and by the Deutsche Forschungsgemeinschaft under grant No. 596/17-1 (W. St.).

References

Athay, R.G., Lites, B.W.: 1972, *Astrophys. J.* **176**, 809
Auser, L.H., Heasley, J.N.: 1976, *Astrophys. J.* **205**, 165
Auer, L.H., Heasley, J.N., Milkey, R.W.: 1972, *Kitt Peak National Obs. Contr. No.* **555**
Blackwell, D.E., Petford, A.D., Shallis, M.J., Simmons, G.J.: 1982, *Monthly Notices Roy. Astron. Soc.* **199**, 43
Chapman, G.A.: 1979, *Astrophys. J.* **232**, 923
Cram, L.E., Rutten, R.J., Lites, B.W.: 1980, *Astrophys. J.* **241**, 374
Delbouille, L., Roland, G., Neven, L.: 1973, *Photometric Atlas of the Solar Spectrum from* λ3000 *to* λ10000, Inst. d'Astrophysique, Liège
Domke, H., Staude, J.: 1973, *Solar Phys.* **31**, 291
Drawin, H.W.: 1966, *Collision and Transport Cross-Sections*, Report EUR-CEA-FC-383, Association Euratom-C.E.A., Fontenay-aux-Roses (revised version 1967)
Drawin, H.W.: 1968, *Z. Phys.* **211**, 404
Drawin, H.W.: 1969, *Z. Phys.* **225**, 483
Frazier, E.N.: 1971, *Solar Phys.* **21**, 42
Frazier, E.N., Stenflo, J.O.: 1978, *Astron. Astrophys.* **70**, 789
Gigas, D.: 1986, *Astron. Astrophys.* **165**, 170
Gingerich, O., Noyes, R.W., Kalkofen, W., Cuny, Y.: 1971, *Solar Phys.* **18**, 347
Gustafsson, B.: 1973, *Uppsala Astron. Obs. Ann.* **5**, No. 6
Hofsäss, D.: 1975, *J. Quant. Spectrosc. Rad. Transfer* **15**, 901
Holweger, H.: 1967, *Z. Astrophys.* **65**, 365
Holweger, H., Müller, E.A.: 1974, *Solar Phys.* **39**, 19
Koutchmy, S.: 1977, *Astron. Astrophys.* **61**, 397
Kurucz, R.L.: 1979, *Astrophys. J. Suppl. Ser.* **40**, 1
Landi Degl'Innocenti, E.: 1976, *Astron. Astrophys. Suppl.* **25**, 379
Lites, B.W.: 1973, *Solar Phys.* **32**, 283
Mäckle, R., Griffin, R., Griffin, R., Holweger, H.: 1975, *Astron. Astrophys. Suppl.* **19**, 303

Mihalas, D., Auer, L.H., Mihalas, B.R.: 1978, *Astrophys. J.* **220**, 1001
Muller, R.: 1975, *Solar Phys.* **45**, 105
Muller, R., Keil, S.L.: 1983, *Solar Phys.* **87**, 243
Owocki, S.P., Auer, L.H.: 1980, *Astrophys. J.* **241**, 448
Pneuman, G.W., Solanki, S.K., Stenflo, J.O.: 1986, *Astron. Astrophys.* **154**, 231
Rachkovsky, D.N.: 1963, *Izv. Krymsk. Astrofiz. Observ.* **30**, 267
Rees, D.E.: 1969, *Solar Phys.* **10**, 268
Ruland, F., Griffin, R., Griffin, R., Biehl, D., Holweger, H.: 1980, *Astron. Astrophys. Suppl.* **42**, 391
Rutten, R.J.: 1987, in *Physics of Formation of* Fe II *Lines Outside LTE*, *IAU Coll.* **94**, ed. R. Viotti, (in press)
Rutten, R.J., Kostik, R.I.: 1982, *Astron. Astrophys.* **115**, 104
Rybicki, G.B.: 1971, *J. Quant. Spectrosc. Radiat. Transfer* **11**, 589
Schmahl, G.: 1967, *Z. Astrophys.* **66**, 81
Schüssler, M., Solanki, S.K.: 1987, *Astron. Astrophys.* (submitted)
Simmons, G.J., Blackwell, D.E.: 1982, *Astron. Astrophys.* **112**, 209
Spruit, H.C.: 1974, *Solar Phys.* **34**, 277
Solanki, S.K.: 1986, *Astron. Astrophys.* **168**, 329
Solanki, S.K., Stenflo, J.O.: 1984, *Astron. Astrophys.* **140**, 185
Solanki, S.K., Stenflo, J.O.: 1985, *Astron. Astrophys.* **148**, 123
Steenbock, W.: 1985, in *Cool Stars with Excesses of Heavy Elements*, eds. M. Jaschek, P.C. Keenan, Reidel, Dordrecht, p. 231
Steenbock, W., Holweger, H.: 1984, *Astron. Astrophys.* **130**, 319
Stellmacher, G., Wiehr, E.: 1973, *Astron. Astrophys.* **29**, 13
Stenholm, L.G., Stenflo, J.O.: 1977, *Astron. Astrophys.* **58**, 273
Stenholm, L.G., Stenflo, J.O.: 1978, *Astron. Astrophys.* **67**, 33
Unsöld, A.: 1968, *Physik der Sternatmosphären*, 2nd. ed. Springer, Berlin, Heidelberg, New York
Watanabe, T., Steenbock, W.: 1986, *Astron. Astrophys.* **165**, 163